JOURNAL OF GEOPHYSICAL RESEARCH, VOL. 97, NO. C3, PAGES 3529–3541, MARCH 15, 1992

Seasonal Variations in the Western Tropical Atlantic: Surface Circulation From Geosat Altimetry and WOCE Model Results

NORBERT DIDDEN AND FRIEDRICH SCHOTT

Institut für Meereskunde an der Universität Kiel, Kiel, Germany

Sea level variations and geostrophic circulation in the western tropical Atlantic are studied in an intercomparison of Geosat altimetry and the World Ocean Circulation Experiment community model effort high-resolution model forced with climatological windstress. Overall, the annual cycles of geostrophic current fields of both products compare very well. Special comparison areas are the western North Equatorial Countercurrent (NECC) and the North Brazil Current (NBC) region. Meridional profiles of zonal velocity anomalies show a seasonal meridional migration of the NECC core centered at 5°N and a weaker eastward maximum during fall at 9°N in both products. The Geosat and model seasonal cycles of the NECC core velocity in the region 35°–45°W are highly correlated and agree with respect to the onset of eastward current acceleration and deceleration in May and December, respectively. Geosat time series from November 1986 to June 1989 show year to year differences, in particular an anomalous early NECC acceleration phase in 1987. In the NBC region 54°–58°W, flow anomalies from both Geosat and the model have two westward maxima, in March and June, which appear to be associated with eastward anomalies further offshore.

1. INTRODUCTION

The near-surface circulation of the tropical Atlantic Ocean is well known to have a strong seasonal cycle. In the western boundary current region, part of the South Equatorial Current (SEC) continues as a western boundary current, the North Brazil Current (NBC), along the northern Brazil and Guyana coasts. Ship drifts and surface drifters [*Richardson and McKee*, 1984; *Richardson and Reverdin*, 1987], as well as numerical ocean circulation models [*Philander and Pacanowski*, 1986; *Schott and Böning*, 1991], indicate that in late summer the coastal surface current separates from the coast at about 5°N and feeds the eastward flowing North Equatorial Countercurrent (NECC), which reaches maximum eastward velocities in late summer. During this retroflection period the continuation of the NBC west of about 55°W is expected to vanish or to have minimum westward transport, whereas in spring it is assumed to continue along the coast and potentially to transport equatorial water into the Caribbean Sea.

As part of the effort to study the seasonal cycle of the western boundary current system, we utilize Geosat altimeter observations. With the beginning of the unclassified Exact Repeat Mission (ERM) in November 1986 the altimeter measurements of the U.S. geodetic satellite Geosat provide the possibility of continuously monitoring variations of sea surface height (SSH). Previous altimetry studies of SSH variability in the tropical Atlantic were carried out by *Menard* [1988] using GEOS III and Seasat altimeter data and by *Carton* [1989] and *Arnault et al.* [1990] using the first year of Geosat data. More recently, *Carton and Katz* [1990] analyzed the 1986–1988 Geosat data and time series obtained from inverted echo sounders (IES) to study seasonal changes in the NECC region.

In this paper we present an analysis of the seasonal variation of SSH and geostrophic velocity for the western tropical Atlantic, derived from more than 2 1/2 years of monthly maps of Geosat SSH anomaly (deviations from a 2-year mean). These results are compared with equivalent products from the eddy-resolving World Ocean Circulation Experiment (WOCE) community model effort (CME) for the Atlantic Ocean which is run at the Institut für Meereskunde in Kiel, Germany (IfM-Kiel), and forced by the seasonally varying climatological wind stress of *Hellerman and Rosenstein* [1983]. An evaluation of the model circulation in the upper layers of the western tropical Atlantic is presented by *Schott and Böning* [1991]. Here we use the model fields of surface pressure and geostrophic velocity for comparison with the altimeter observations.

The intent of the paper is to compare altimetry and model results in order to assess the range of agreement between both products, in particular of seasonally fluctuating spatial circulation patterns, for mutual verification. This will be done comparing the climatologically forced model results with a mean seasonal cycle from 2 years of the altimeter observations. A further characteristic of the seasonal circulation cycle is the interannual variability, which is shown to be clearly present during the altimeter observation period from the end of 1986 through mid-1989.

Other observational data of the seasonal cycle with large spatial coverage in the tropical Atlantic are the climatological data sets of ship drifts [*Richardson and McKee*, 1984] and of dynamic topography [*Merle and Arnault*, 1985]. The ship drift data are used here for comparison in the NECC region. The coarse resolution (4° longitude × 2° latitude) of the dynamic topography data, however, does not well resolve the spatial circulation patterns of interest in our study. This is also obvious from the variability patterns of the dynamic topography data showing considerably less spatial structure than the SSH variability of the first year Geosat data [*Arnault et al.*, 1990]. Thus equivalent observational data for further verification are rare, and the main focus is on altimeter-model comparison.

This paper is organized as follows: After a description of the method used for the analysis of Geosat data and of the numerical model output, we present the results comparing both data sets. There we first show large-scale distributions

Published by the American Geophysical Union.

Paper number 91JC02860.
0148-0227/92/91JC-02860$05.00

10.1029/91JC02860

of seasonal SSH changes and present statistics including the harmonic component of the annual cycle. Subsequently, maps of the geostrophic velocity anomalies north of the equator and of the seasonal characteristics of surface circulation are presented. Finally, we discuss some details of the annual cycles of the western NECC regime (35°–45°W) and of the NBC regime (50°–60°W).

2. Data and Methods

2.1. *Altimeter Data and Analysis*

The Geosat altimeter data analysis of this study covers a period of 2 years, from November 1986 through October 1988 in the region 10°S–30°N and 70°W–20°W, and another 8 months through June 1989 in the NECC region. During the 2-year period the 17.05-day repeat cycle of the Geosat orbit provided 43 sea level profiles along each ground track. The spatial coverage of data is composed of ascending and descending tracks with zonal separation of 164 km at the equator.

In a first processing step the altimeter data from the geophysical data records (GDR) [*Cheney et al.*, 1987] were checked for quality using the rms of the 1-s averages of height H, significant wave height (SWH), and automatic gain control (AGC). Only data satisfying the following quality criteria were used: rms (H) < 10 cm, rms (SWH) < 25 cm, rms (AGC) < 0.2 dB, and SWH < 10 m. These values are based on experience in handling the data and eliminate obviously spurious data. The corrections supplied with the GDR for path delays in the ionosphere and in the dry and wet troposphere (from the Fleet Numerical Oceanographic Center (FNOC) model) as well as height corrections for solid Earth and ocean tides were applied. For sea state bias correction a value of 2% of SWH [*Cheney et al.*, 1987] was used and sea level changes due to local atmospheric pressure changes were corrected assuming isostatic ocean response.

For each track sampled at 6.8-km intervals a collinear analysis [*Cheney et al.*, 1983] was applied using 43 repeats (2 years) to estimate the temporal mean sea level (including the geoid). To avoid a bias of the mean estimate introduced at data gaps due to the 4 m rms orbit error, the determination of the mean sea level proceeded as follows: the alongtrack signal of an arbitrary reference repeat with minimum data gaps was selected as a first guess of the mean sea level and subtracted from each individual repeat, and then the orbit error was removed from each difference signal using a least squares quadratic polynomial and the ensemble mean over all difference signals, i.e. the mean relative to the reference repeat, plus the reference signal was used as the final estimate of mean sea level. The collinear analysis then proceeded as usual: subtraction of the mean sea level from the altimeter signal eliminated the geoid but also the SSH gradients associated with the mean circulation. For orbit error correction [*Cheney et al.*, 1989] a least squares quadratic polynomial over up to 40° of latitude was subtracted from each individual repeat. For tracks shorter than 1000 km, only bias and trend were removed. The residual SSH will be referred to as SSH anomaly, i.e., the deviation from a temporal mean.

The alongtrack data were then filtered with a 70-km running median filter and subsampled at 20-km intervals. For the interpolation in space and time onto 1° × 1° monthly maps, centered on the fifteenth of each month, an optimal interpolation objective analysis [*Bretherton et al.*, 1976] was used. For the algorithm provided by P. De Mey [*De Mey and Menard*, 1989], correlation scales of 300 km and 30 days, inferred from the dominant scales of alongtrack SSH anomaly structures, were chosen; for each grid point, only data within radii of 600 km and 15 days were considered. In regions of low variability the minimum temporal variance of the input data was about 15 cm^2 (with the annual frequency filtered out) and was considered to represent the SSH random error variance, resulting from instrument noise, unresolved process variance, and random errors of the corrections. This value corresponds to typical error-process variance ratio of 30%, which was used for the objective analysis. Error maps from the objective analysis procedure indicate 20–30% random error of the SSH anomaly maps.

The variability of tropospheric water vapour in the tropics may introduce systematic errors due to inaccurate FNOC water vapor corrections [*Emery et al.*, 1990]. The large-scale part of this error is removed by long-wavelength filtering of the altimeter data, and some high-frequency part is reduced by objective mapping, but residual correction errors can contaminate the monthly altimetric SSH maps. During the revision of this paper, water vapor corrections from special sensor microwave imager (SSM/I) data of the Defense Meteorological Satellite Program (DMSP) were made available to us by W. Emery [*Emery et al.*, 1990] for a 1-year period starting in July 1987. The rms difference for the monthly SSH anomaly maps using FNOC and SSM/I corrections, respectively, was 1–2 cm except for some regions east of 50°W near the equator and near 10°N with 2–3 cm rms differences.

Some information on Geosat SSH accuracy in the tropics has been gained recently from comparison with in situ data. *Cheney et al.* [1989] used 14 tide gauge time series in the tropical Pacific Ocean for comparison with Geosat time series over 18 months and found a rms difference of 3–4 cm, based on monthly mean data and space scales similar to our monthly maps. For a record length of 4 years the difference, adjusted to have zero mean for the first year only, was increased to about 5 cm rms due to errors on the long time scales [*Miller and Cheney*, 1990]. From there, for our SSH-anomaly maps referenced to a 2-year mean an error of 4 cm is assumed. From comparison with six IES time series in the Atlantic NECC region, *Carton and Katz* [1990] estimate a 6-cm error, based on 10-day-resolution altimeter time series. For monthly maps this error is likely to be smaller owing to less high-frequency content; using the same spatial averaging as Carton and Katz at the IES positions, we found the signal strength of SSH anomaly time series from our monthly maps to be 30% lower than those of *Carton and Katz* [1990, Table 1]. Assuming the same reduction for the error, this would indicate a 4-cm error for our anomaly maps. These errors also include the effect of attenuation of the large-scale part of oceanic variability due to the long-wavelength orbit error correction.

In shallow water the temporal SSH variability of the alongtrack data increased significantly toward the coast. This increase of variability was most likely due to tide correction errors on the continental shelf, which off Guyana is typically 200 km wide with bottom topography rising from 2000 m to 500 m within 50 km. The increase of SSH variability was found to be restricted to depths of less than

500 m. This result was also found for tracks crossing the Demerara plateau at 52°–55°W with a continental slope rising from 2000 m to 500 m over 180 km. Thus for the study of the NBC seasonal cycle near the continental shelf, we excluded data at depths less than 500 m before performing the collinear analysis. Errors due to cross-track geoid gradients and cross-track displacement of repeated ground tracks (0.6 km rms) are small. Assuming that geoid gradients in the area are resolved by the one-twelfth degree resolution of mean sea surface maps of *Marsh et al.* [1984], this random error is estimated to be typically less than 2 cm, i.e., below the noise level of the altimeter signal.

2.2. *Ocean Model Data*

The model data used for comparison with altimetry results are products of the high-resolution WOCE model developed by *Bryan and Holland* [1989]. The primitive equation model covering the Atlantic Ocean between 15°S and 65°N has a resolution of one-third degree in latitude, two-fifths degree in longitude, and 30 levels in the vertical. The vertical spacing of the uppermost three layers is 35 m, 37 m, and 40 m. The model was run at IFM-Kiel as part of the WOCE community model effort (CME) by *Böning et al.* [1991]. We used results from a model run with vertical friction of 10 $cm^2\ s^{-1}$, lateral biharmonic friction with coefficient of $-2.5 \times 10^{19}\ cm^4\ s^{-1}$, and forcing with seasonal wind stress [*Hellerman and Rosenstein*, 1983]. The influence of friction parameterization is discussed by *Böning et al.* [1991].

The seasonal cycle of this model is described by *Schott and Böning* [1991]. The model produces a meandering NECC during July to December with two current cores, one at about 5°N and a weaker one at about 9°N. The meanders of about 900-km wavelength are very stable and are reproduced year after year in the same location. In December the model NECC suddenly collapses, and weak westward flow occurs in the western NECC regime. Along the northern Brazil–Guyana coast the model does not produce a continuous surface boundary current in connecting the cross-equatorial flow regime with the inflow region of the eastern Caribbean, in either season. A relevant result for this study was the low amount of interannual variance (typically less than 10% of the annual cycle variance) found in the tropical Atlantic part of the model which permits us to use fields of an individual model year for extraction of the typical annual cycle in the following. This deterministic behavior in the tropics is in contrast to the subtropical western Atlantic, where the climatologically driven model produces strong interannual variations, which may even mask the annual cycle (e.g., in the Antilles current region [*Böning et al.*, 1991]).

The surface pressure gradient of the model was calculated from the prognostic variables of the rigid lid model using the horizontal momentum equations. The surface pressure field was then derived from the gradient field; the integration constant is given by the condition of zero average surface pressure over the model domain in order to satisfy conservation of mass. The surface pressure fields of model year 24 at the middle of each month were used to evaluate the model SSH and to derive geostrophic surface velocity by assuming geostrophic balance of the pressure gradient. The 12 monthly maps were spatially averaged over 1° × 1° boxes, and the annual mean was subtracted for comparison with the monthly SSH and velocity anomaly fields from altimetry.

3. COMPARISON OF ALTIMETER AND MODEL MAPS

3.1. *Seasonal Cycle of Sea Surface Height*

Two monthly maps of SSH anomaly, for April and October 1987 (Figure 1), are selected to display the principal pattern of SSH variations: they show characteristic large-scale structures with remarkable similarities between altimetry and model maps. Most prominent is the contrast between zonal ridges and troughs: in April a positive anomaly between about 5°N and 15°–20°N extends zonally from 20°W to 60°W (Figures 1*a* and 1*c*). South of it a negative anomaly extends zonally from 25°W to 50°W. Half a year later, in October, the high and low zonal ridges are reversed (Figures 1*b* and 1*d*). The strong meridional gradients between these positive and negative anomalies indicate high zonal geostrophic velocity anomalies, most significant in the NECC region centered at about 5°N. Also, between 45°W and 60°W the altimetry maps show a band of SSH anomaly contours parallel to the northern Brazil and Guyana coasts with offshore slopes reversing sign from April to October. Superimposed on the spatial structure described above are features with a typical scale of a few hundred kilometers. This scale is not imposed by the objective analysis scheme, but it is also obvious in the alongtrack SSH signals.

For the model seasonal cycle, year to year differences are negligible. Thus in order to suppress interannual variability present in the Geosat data, we use the mean seasonal cycle formed by averaging the altimeter maps by months over the 2-year period November 1986 to October 1988. The seasonal SSH variations show maximum rms values of 6–8 cm in the NECC region (Figure 2*a*). Note that variability based on alongtrack SSH data is slightly higher, since objective mapping removes some high-wavenumber variability and the averaging by months removes part of the interannual variability. For the model (Figure 2*b*) the maximum variance occurs near the coast at 11°N, north of the NBC–NECC retroflection region. A weaker zonal band of a relative maximum of SSH displacements with rms values of 4–6 cm is associated with the NECC, and another branch of similar SSH variance extends into the North Equatorial Current (NEC) regime from about 11°N, 40°W, to 15°N, 30°W, i.e., less zonally orientated than in the altimeter maps.

From their analysis of ship drift data, *Richardson and Walsh* [1986] found that the annual harmonic of surface currents represents more than 80% of the total variance, while the semiannual harmonic contributes less than 20% in most of the western tropical Atlantic. Therefore in the following we compare annual cycles of Geosat and model products in terms of the annual harmonic.

The amplitude map of the annual harmonic from 2 years of altimeter data (Figure 3*a*) shows maximum amplitudes along 3°N at the southern boundary of the NECC in the region 25°W to 45°W, where the annual harmonic accounts for more than 90% of the total variance (Figure 3*b*). Between this maximum and a zonal band of minimum annual SSH fluctuations at 7°N, a band of maximum gradients in the amplitude of SSH fluctuations indicates maximum velocity fluctuations of the NECC at about 5°N. A weaker maximum exists along 12°N at the northern boundary of the NECC and along the northern Brazil–Guyana coast with explained variance of more than 60%. For the model data (Figures 3*c* and 3*d*) the largest annual harmonic SSH signal is concentrated along 12°N, where the annual variance contributes about 90% to

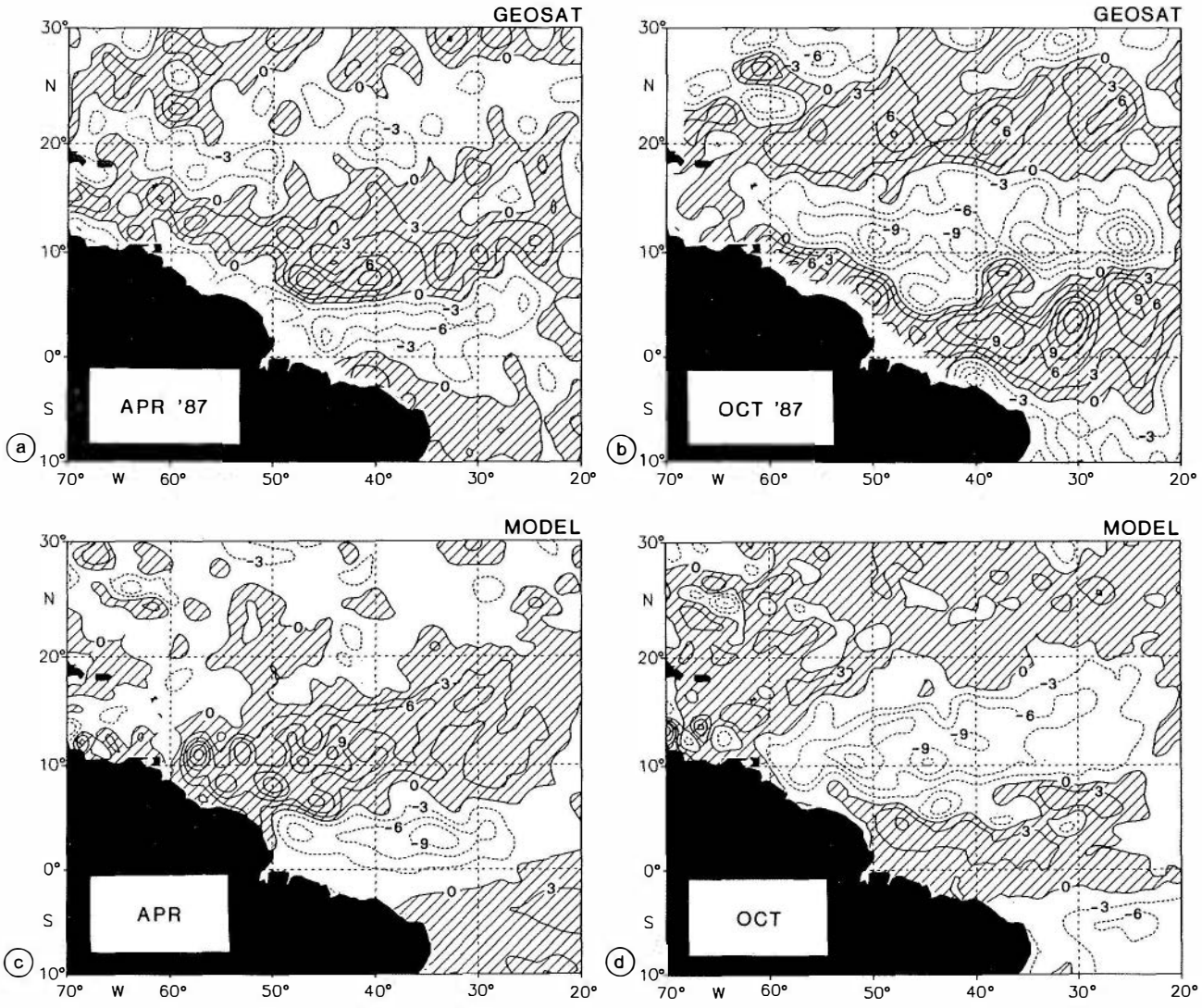

Fig. 1. Sea surface height anomaly: 1° × 1° monthly maps of Geosat altimetry for (*a*) April and (*b*) October 1987 and model for (*c*) April and (*d*) October. The contour interval is 3 cm and positive anomalies are hatched.

the total variance, and in this case the maximum at the southern NECC flank is smaller. The large-scale structure of annual harmonic variability with zonal bands centered at about 3°N and 12°N and a relative minimum along 7°N is similar in both model and altimetry maps. Also, since in regions of large total SSH variability (Figure 2) generally more than 60% of the variance is explained by annual harmonic variance, these regions roughly coincide with regions of large annual SSH variability.

3.2. *Seasonal Cycle of Geostrophic Velocity*

The anomaly of velocity north of 2°N is derived from SSH anomaly for both the altimeter and model data assuming geostrophic balance of the surface pressure gradient. Since the main focus of this paper is on the western boundary current region and its connection with the NECC, the results are discussed west of 35°W only.

The velocity map of the Geosat mean seasonal cycle in April (Figure 4*a*) shows strong westward velocity anomalies in the NECC between 4°N and 6°N and in the NBC region off the shelf west of 50°W. This flow pattern is more clearly represented by the annual harmonic component of geostrophic velocity: in the annual harmonic signal for April (Figure 4*b*), most mesoscale features of Figure 4*a* are filtered out. Half a year later in October, the annual harmonic signal is identical, except that current directions are reversed. As will be seen later from the time series, April is approximately the month at which the westward velocity anomaly in the NBC region west of 50°W and in the western NECC approaches a maximum.

For comparison of the altimetric geostrophic velocity anomaly with model results, we first discuss the annual mean of the surface velocity in the WOCE model. The mean geostrophic velocity field (Figure 5*a*) is dominated by the eastward NECC with maximum velocity between 4°N and 6°N and a region of weak eastward mean flow up to 11°N. Part of the NBC near 50°N turns offshore into the NECC, and part of it continues westward along the coast with decreasing strength. The difference between the absolute surface velocity and the geostrophic velocity (derived from the surface pressure gradient) is shown in Figure 5*b*. Most of the difference can be attributed to the wind-driven currents

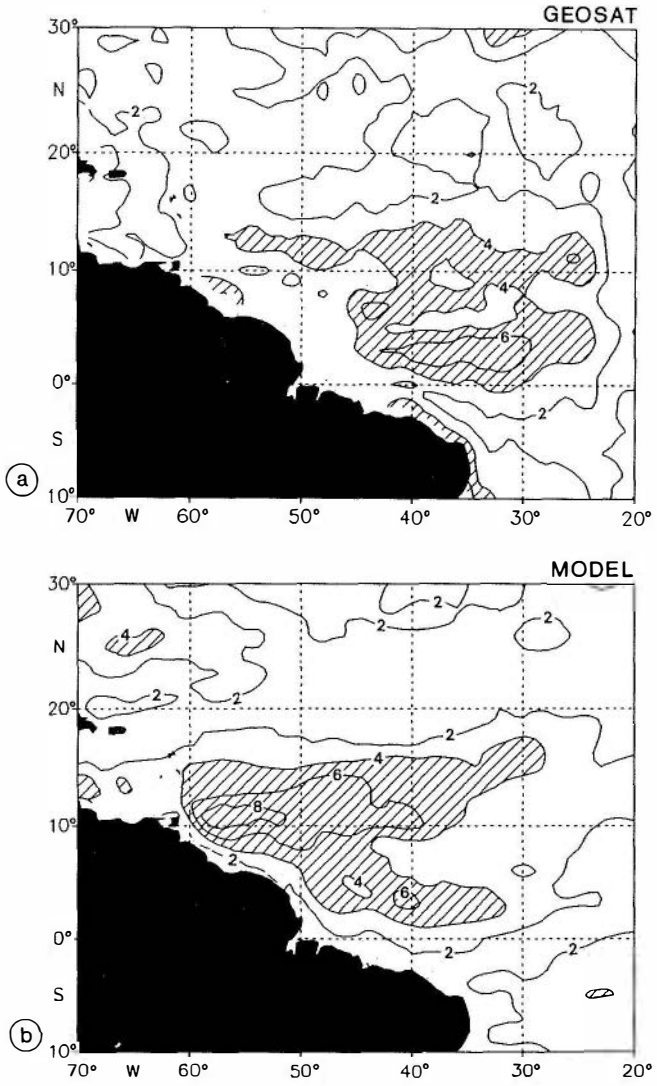

Fig. 2. Sea surface height rms variability, based on time series from monthly maps for (*a*) Geosat mean seasonal cycle and (*b*) model seasonal cycle. The contour interval is 2 cm; the hatched area indicates rms > 4 cm.

in the model surface layer of 35-m thickness: this is obvious from comparison with the Ekman transport velocity (mean over 35-m layer) derived from the Hellerman and Rosenstein wind stress (Figure 5*c*). Thus to obtain the absolute surface velocity field, as measured by ship drifts and drifters, the Ekman transport in the model surface layer, which is predominantly northward, has to be added. In the following, however, we use only geostrophic model velocities for the comparison with altimetry. We should note here that in the western boundary current region the assumption of geostrophic balance of the pressure gradient may not be fully satisfied owing to nonlinear velocity components. Maximum deviations from the geostrophic balance are estimated to be 20% in the retroflection region 48°–50°W (Figure 5), where nonlinear radial acceleration is about 20% of the Coriolis acceleration, based on 50 cm s^{-1} azimuthal velocity difference over 200 km.

The annual harmonic of geostrophic velocity from altimeter and model data for April (Figures 4*b* and 6) shows striking similarities. In both maps the annual cycle of the NECC between 35°W and 45°W is characterized by a band of strong zonal flow anomaly, which in April (October) is westward (eastward) and confined between 4°N and 6°N. At the coast, this westward anomaly splits up into a northwestward component and into a strong southward and then eastward return flow anomaly along 2°N. South of 5°N the strong southeastward velocity anomaly parallel to the coast in both altimetry and model maps of April indicates a reduced strength of the northwestward boundary current in spring. The pronounced meander pattern of the model NECC, also apparent in the model mean flow, is not found in the Geosat annual harmonic velocities.

In the NBC region between 50°W and 60°W the westward geostrophic velocity anomaly in April is strongest between 9°N and 11°N for the altimeter data. In the model map the NBC anomaly is located closer to the coast and predominantly westward, and centered at about 8°N. West of 58°W, the velocity anomaly in both maps gains a northward component under the influence of the Antilles Islands.

The amplitude of the annual harmonic of zonal flow is shown in Figure 7. The shading indicates regions in which the annual harmonic explains more than 50% of the total variance. The altimeter map (Figure 7*a*) shows maxima in the NECC centered at about 5°N and in a zonal band further west centered at 10°N. North of about 12°N in the NEC region annual fluctuations generally have amplitudes of less than 4 cm s^{-1}. The model values for annual harmonic variance (Figure 7*b*) are typically larger over the whole map, but the average of amplitudes over meander crest and trough of the NECC corresponds to the NECC maximum of the Geosat results (see also next section). The model NECC region of large annual zonal current fluctuations extends further westward than in the altimeter data.

The directions of vector fluctuations are displayed by the principal axes of the current ellipses of the rotating annual harmonic velocity vector (Figure 8). Annual altimeter-derived current fluctuations are predominantly zonal in the strong current region of the NECC and parallel to the coast in the NBC region (Figure 8*a*). The meander pattern of the model NECC is also obvious in the annual harmonic of velocity fluctuations (Figure 8*b*). The phase maps of maximum annual harmonic amplitude in Figure 9 indicate the month in which the velocity vector is aligned with the major axis and has an eastward component. In most of the NECC and NBC regions, the eastward anomaly reaches a maximum between September and November (shaded in Figure 9) for both altimetry and model data. North of about 12°N the small annual fluctuations in the NEC reach eastward maxima between February and May. The major axis velocity fluctuations are, in general, significantly larger than those along the minor axes; i.e., the velocity fluctuations of annual period have a preferred orientation. In several regions the major axes are aligned with the mean flow direction as inferred from comparison of model principal axes (Figure 8*b*) with the model mean flow (Figure 5*a*). Preferred fluctuations in the mean flow direction are consistent with annual modulation of the current strength as well as with a current migration normal to its axis.

In summary, the maps of the annual harmonic of geostrophic velocity derived from altimetry and model data show consistent spatial patterns of the annual current variations in the NECC and the NBC north of the equator.

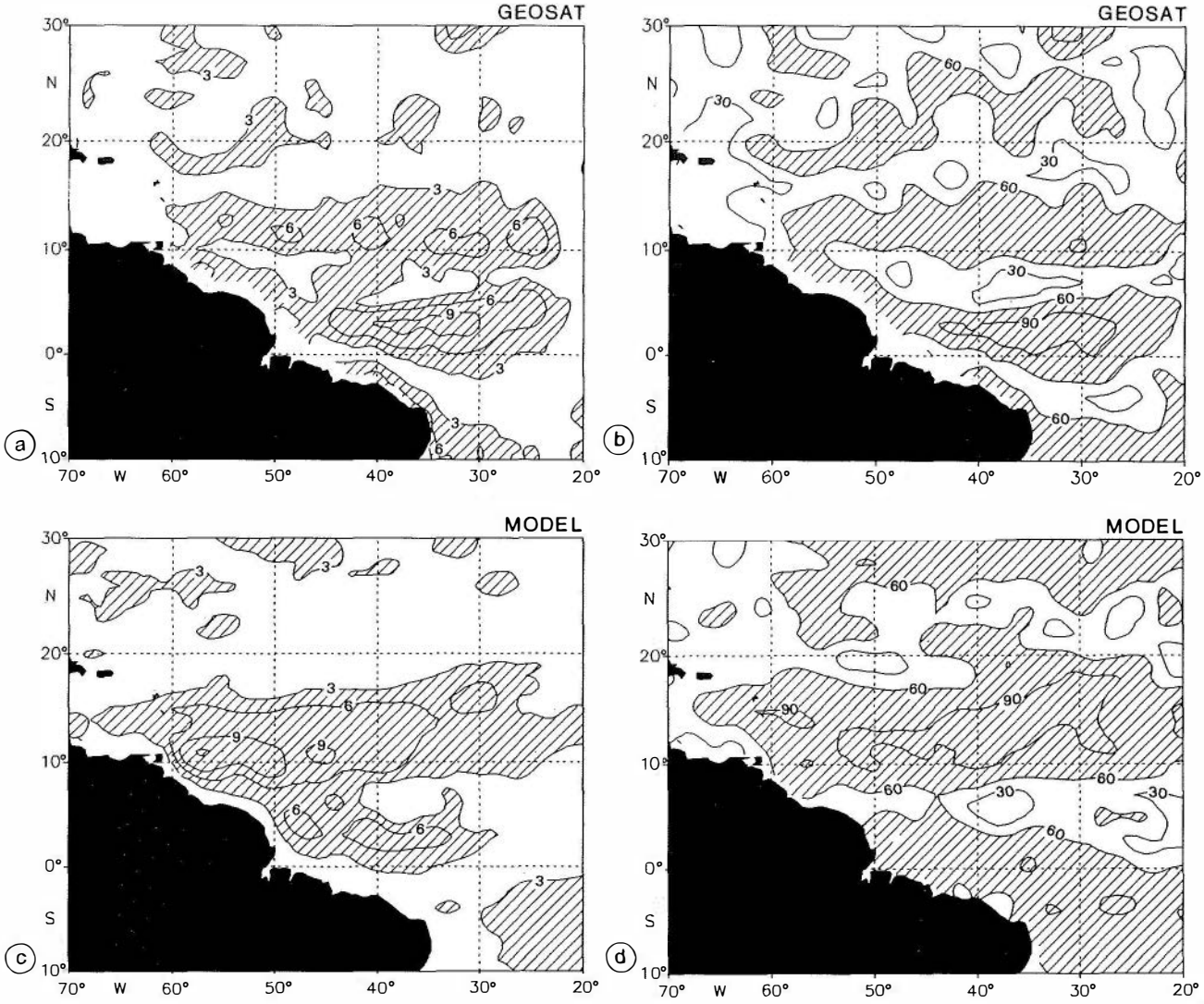

Fig. 3. Annual harmonic cycle of sea surface height: (*a*) amplitude and (*b*) explained variance for Geosat, and (*c*) model amplitude and (*d*) model explained variance. The contour interval is 3 cm and 30%, respectively.

4. Seasonal Cycle of the Western NECC

In order to show principal features of the western NECC, the zonal geostrophic velocity anomaly for altimetry and WOCE model was averaged between 35°W and 45°W. The meridional structure and temporal development is displayed in the latitude-time plot of Figure 10. The Geosat data coverage in this region was good enough to extend the data analysis for 8 more months, through June 1989 (Figure 10*a*). The seasonal cycles of individual years clearly show year to year differences, but nevertheless all the prominent features of individual years are represented in the mean seasonal cycle of the first 2 years (Figure 10*b*). Maximum fluctuations of the NECC are located near 5°N. The eastward velocity increase from spring to fall is about 90 cm s^{-1} in 1987 and 70 cm s^{-1} in 1988. This interannual variability will be discussed later. For the mean seasonal cycle the spring to fall increase is 75 cm s^{-1}. Strong in-phase fluctuations of the NECC are essentially confined between 3°N and 7°N. The model results (Figure 10*c*) show a similar meridional and temporal structure with a reduced contrast between the minimum and maximum NECC anomalies in spring and fall. The closest resemblance is found to the 1988 and 1989 altimeter observations.

Meridional profiles of zonal velocity anomaly are shown in Figure 11 for the altimetry mean seasonal cycle and for model data. In both products the NECC velocity anomaly is westward during January to June. In July the NECC velocity anomaly reverses to eastward and its maximum moves northward, starting in October. Taking into account the model annual mean flow (at the right margin of Figure 11*b*), this indicates a northward shift of the NECC axis from 4.5°N in October to 6°N in January. The northward propagation of the eastward velocity anomalies is more obvious from the latitude-time plot of Figure 10: it is seen for all Geosat winter seasons in the latitude band 5°–8°N with a northward phase velocity component of 4 cm s^{-1} and in the model data with about 3 cm s^{-1} phase velocity.

In the band 4°N to 7°N the model geostrophic current is eastward all year. Further south, Geosat and model anomaly profiles show a rapid change of geostrophic velocity between June and August, indicating a strong increase of the westward SEC velocity. North of the NECC core the anomaly

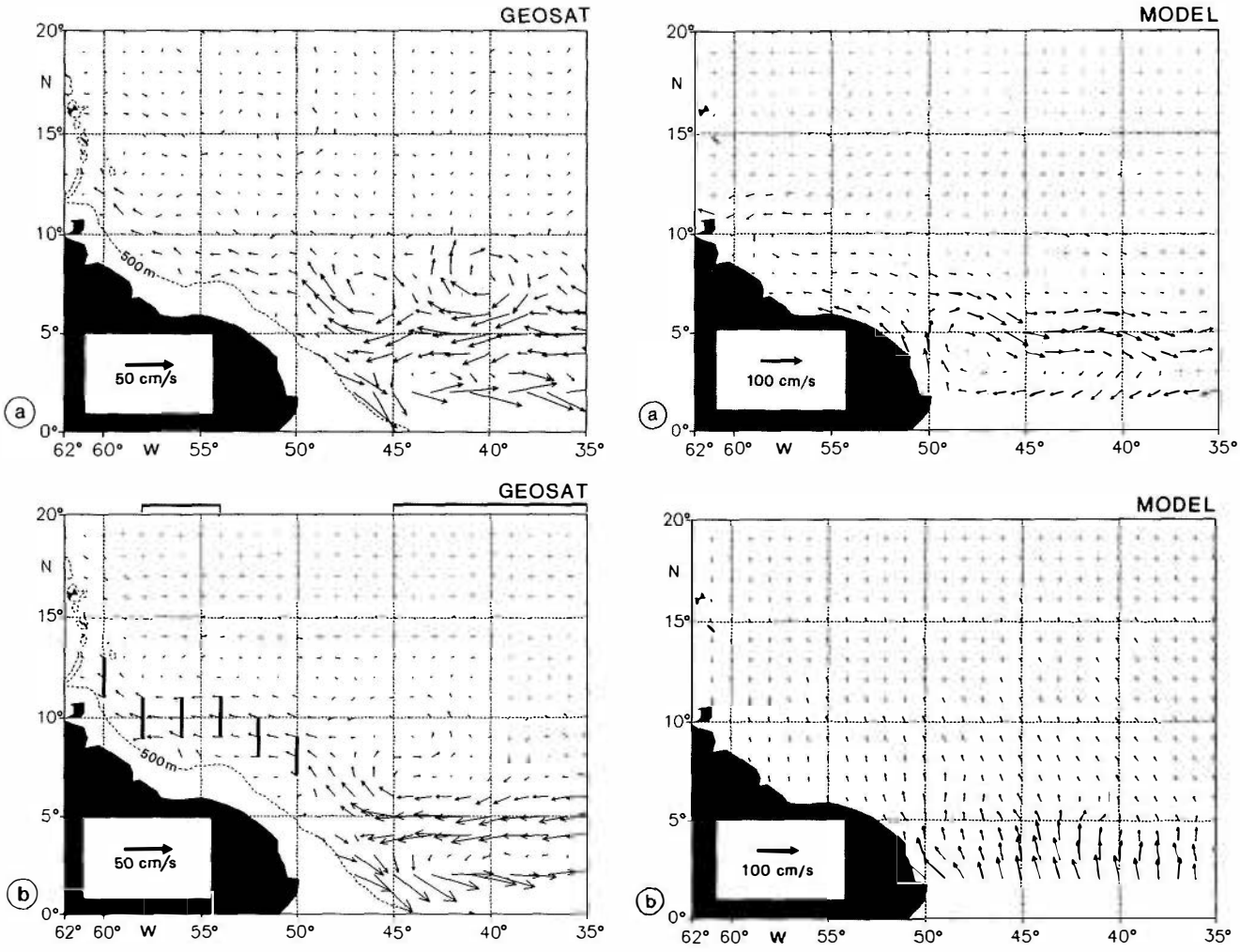

Fig. 4. (*a*) Geostrophic velocity anomaly and (*b*) annual harmonic of geostrophic velocity in April from Geosat mean seasonal cycle. Note in Figure 4*b* that October vectors have the same magnitude in opposite direction. Heavy bars indicate averaging ranges for the NECC in Figures 10–12 and for the NBC in Figures 13 and 14.

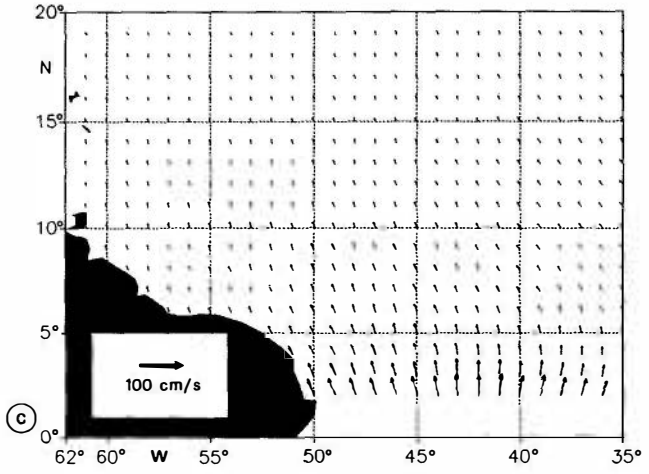

Fig. 5. Annual mean of surface velocity. (*a*) Model geostrophic velocity. (*b*) Upper layer (thickness 35 m) model current: absolute velocity minus geostrophic velocity. (*c*) Mean Ekman current in 35-m layer (from Hellerman and Rosenstein wind stress for Ekman depth of 35 m).

profiles of both products exhibit a relative minimum and a secondary maximum of eastward anomaly at about 9°N, starting in late summer. Adding the anomaly to the geostrophic model mean flow results in a total geostrophic velocity profile with the same double peak structure during the phase of strong eastward flow. The Geosat observations confirm the double peak structure of the NECC with maxima at 5°N and about 9°N during fall, although less pronounced, and meridionally more strongly smoothed. The smoother appearance of Geosat profiles is mainly due to differences between the two averaged Geosat years (see Figure 10*a*). North of 11°N the model velocity profiles continue with several more reversals suggesting a rich meridional wave structure, not present in the altimetry data. This seems to indicate that the wave content of the model may be unrealistically high.

The climatological surface currents derived from ship drift observations by *Richardson and McKee* [1984] were also used for comparison. We here reproduce Figure 5*b* of their paper after having subtracted the annual mean zonal velocity (showed at right margin) from each monthly profile (Figure 11*c*). These profiles include the Ekman drift velocity driven by local wind stress. Nevertheless, the comparison with altimeter geostrophic velocity shows agreement in many details. Between January and June the phase and the merid-

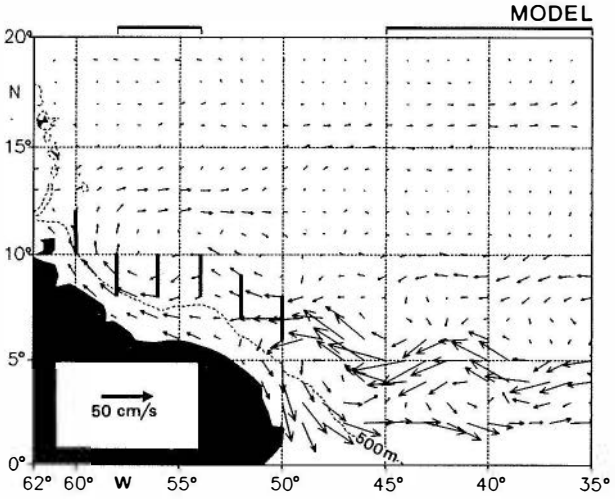

Fig. 6. Annual harmonic of geostrophic velocity in April from model. For comments, see legend of Figure 4*b*.

ional position of minima and maxima coincide very well. Largest deviations occur from August through October, when the ship drifts show a positive eastward anomaly in the NECC over a larger latitude range and the position of maximum anomaly is shifted northward. Also, the contrast between maximum and minimum anomaly of each monthly ship drift profile is reduced owing to the meridional smoothing effect of climatological averaging.

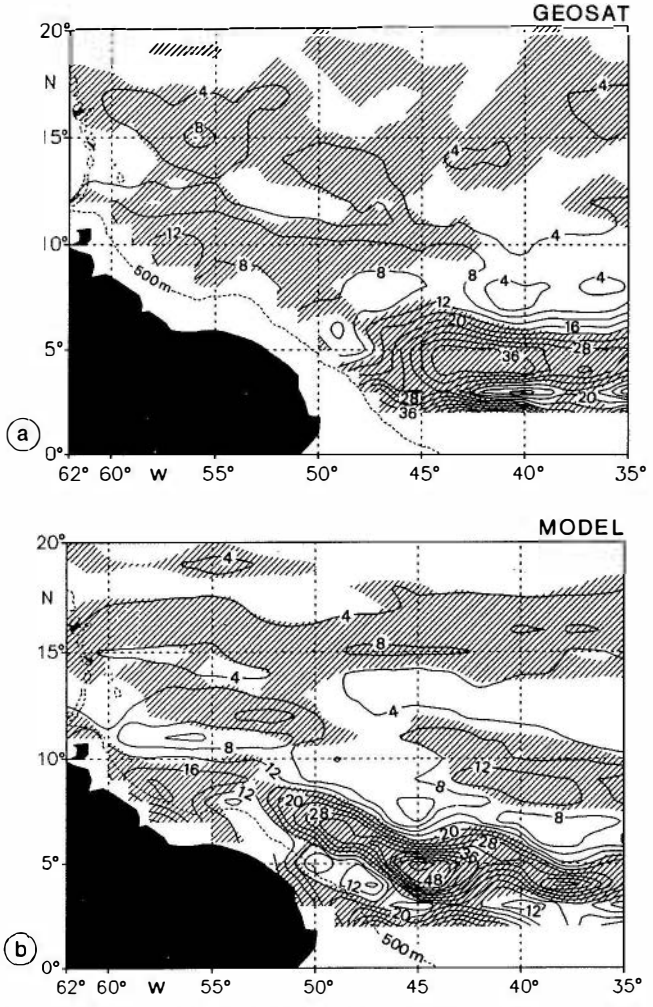

Fig. 7. Amplitude of the annual harmonic of zonal geostrophic velocity, for (*a*) Geosat altimetry and (*b*) model. The contour interval is 4 cm s^{-1}. In the hatched regions the annual harmonic variance accounts for more than 50% of the total variance.

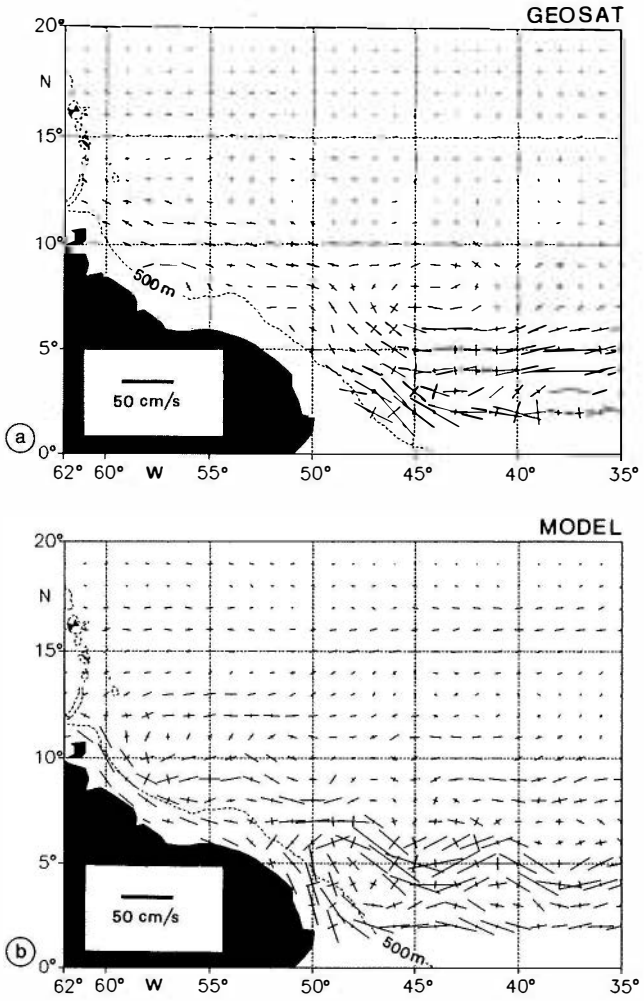

Fig. 8. Principle axes of annual harmonic geostrophic velocity, for (*a*) Geosat altimetry and (*b*) model.

The time series of velocity fluctuations in the core of the NECC, meridionally averaged between 4°N and 6°N (Figure 12), shows the deviation from an annual harmonic cycle. For the Geosat mean seasonal cycle the acceleration period from April through November (8 months) is significantly longer than the 4-month period of relaxation of eastward flow starting in December. The increase of the eastward current is retarded during August and September. This slow and interrupted increase and fast decrease of eastward velocity may possibly be a systematic feature of the NECC seasonal cycle. For the geostrophic model currents the spring to fall increase of about 45 cm s^{-1} is smaller than the 60 cm s^{-1} increase for altimetry and the maximum eastward flow is almost constant between July and December. The onset of acceleration and deceleration in May and December, respectively, coincides well with the Geosat observations, in particular during the last 2 Geosat years (see also Figure 10*a*). The rms difference between Geosat and model velocities in the NECC core is 7 cm s^{-1} (Table 1); i.e., the variance of the difference is only about 10% of the signal variance. The rms amplitude of Geosat seasonal velocity

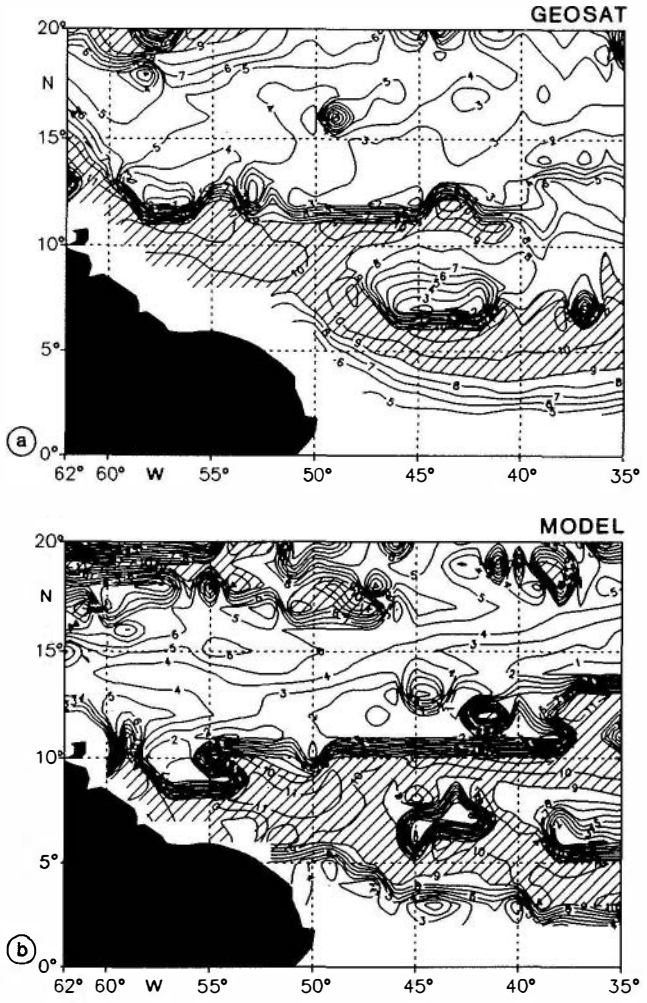

Fig. 9. Phase of annual harmonic geostrophic velocity for (*a*) Geosat altimetry and (*b*) model. Contours show the months (1–12 denote January–December) at which the current vector reaches maximum amplitude in easterly major principle axis direction (see Figure 8). The hatched area indicates the maximum between September and November.

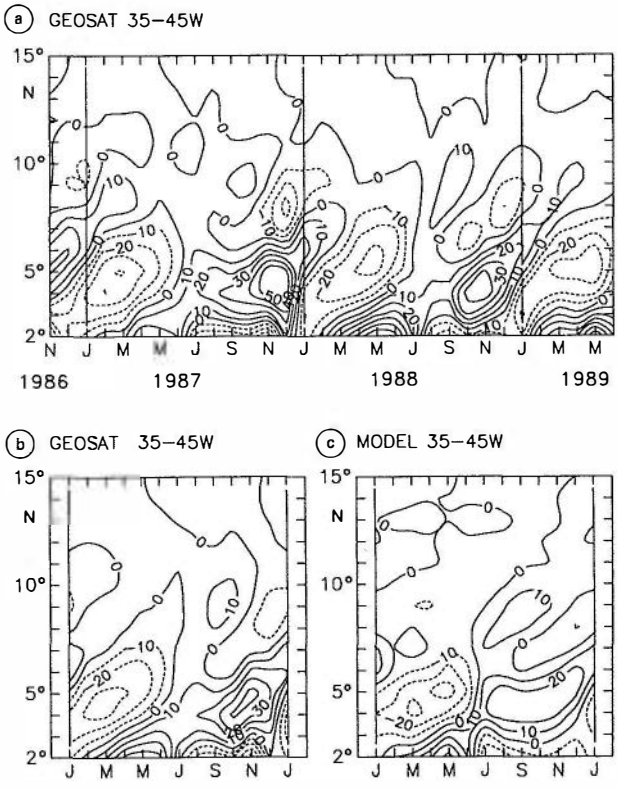

Fig. 10. Latitude-time plot of zonal geostrophic velocity anomaly in the western NECC, 35°–45°W: (*a*) Geosat altimetry, November 1986 to June 1989; (*b*) Geosat, mean seasonal cycle; and (*c*) model, seasonal cycle. The contour interval is 10 cm s^{-1}.

fluctuations is slightly larger (12%), and the correlation with the model velocities is high (0.95). Table 1 further indicates the very good agreement between Geosat and model results for amplitude and phase of the annual harmonic cycle (dotted line in Figure 12).

The interannual variability of the observed seasonal NECC fluctuations is characterized by an early decrease of the eastward velocity component until February 1987, then an early onset of the acceleration phase in March 1987, whereas in the 2 following years it starts 2 months later, in May. The longer acceleration phase in 1987 leads to a significantly larger spring to fall increase of eastward current in 1987 (about 80 cm s^{-1}) than in 1988 (about 55 cm s^{-1}). Therefore the 1987 period seems to be anomalous as compared with the period 1988 to mid-1989: the last 2 years show closer resemblance to each other and to the model seasonal cycle (see also Figures 10*a* and 10*c*).

5. Seasonal Cycle of the NBC

Model results (Figure 8*b*) show the retroflection region of the NBC into the NECC to extend westward to 52°W on the continental shelf. Off the shelf and north of 6°N, annual fluctuations in the westward continuation of the NBC are predominantly zonal, as can be seen from the altimetry and model maps of Figure 8. To describe the seasonal cycle, the zonal velocity anomaly is meridionally averaged over 2° (see Figures 4*b* and 6) centered at the meridional peak of the annual harmonic velocity. As compared with altimeter observations, the model peak is located about 1° further south, i.e., closer to the coast.

The boundary current time series (Figure 13) show seasonal geostrophic velocity fluctuations of typically 20 to 30 cm s^{-1} decreasing from east to west. The annual harmonic velocities from altimetry (Figure 13*a*) indicate maximum westward anomaly in April in the 50°–52°W band and about a month later at 58°W–60°W, just east of the Lesser Antilles. For the model (Figure 13*b*) the annual mean geostrophic flow across the selected sections is eastward (except for 60°W), but its magnitude is smaller than the annual harmonic amplitude and thus the NBC flow is westward during spring. The annual harmonic velocities have westward maxima occurring 1–2 months after those obtained from Geosat and generally have larger amplitudes. In the 54°–58°W longitude range, where geostrophic velocity fluctuations are almost zonal (Figure 8), the agreement between Geosat and model seasonal cycles is substantially improved when Geosat data 1° further offshore and delayed by 1 month are compared with the model data (Table 1, cases a–d): the rms difference decreases to 2.5 cm s^{-1} and thus contributes less than 10% to the variance of the seasonal signal. The Geosat amplitude is 14% smaller, but the seasonal cycles are very well correlated (0.97) and the phases of the annual harmonics

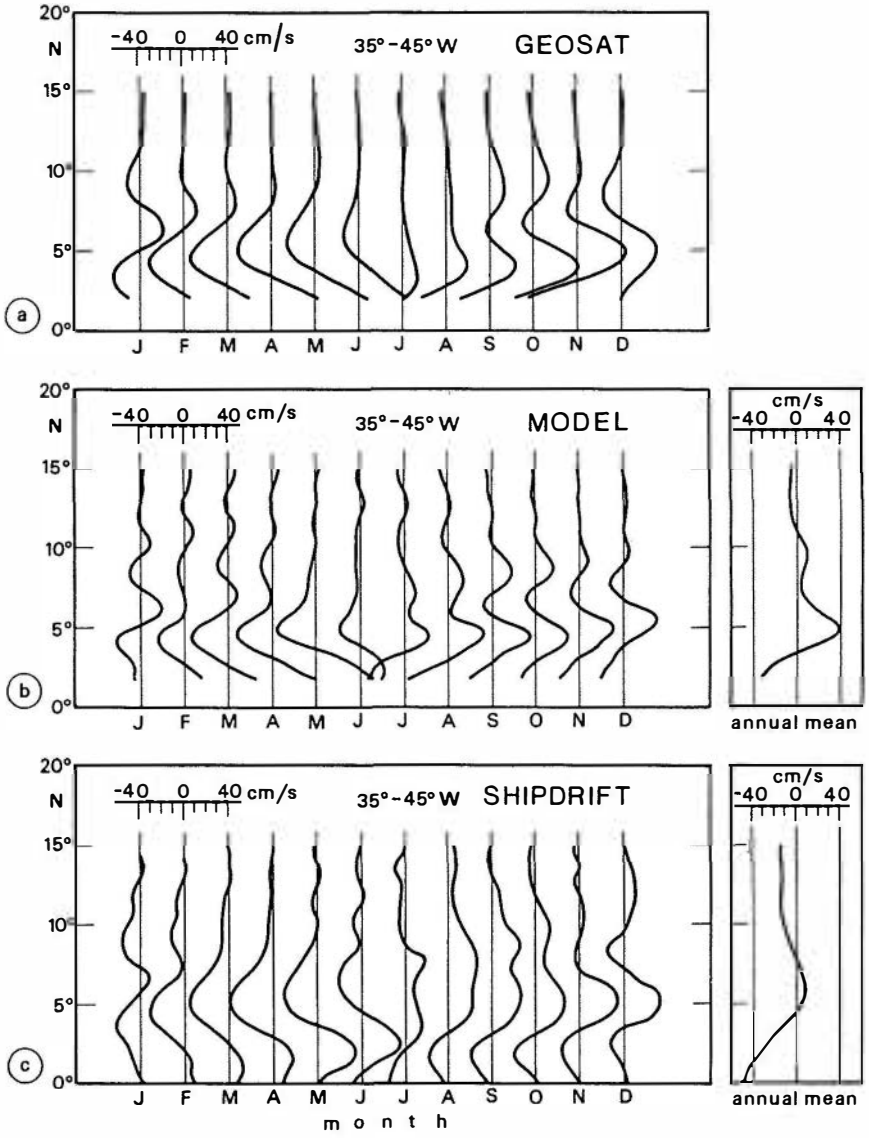

Fig. 11. Profiles of zonal velocity anomaly (NECC, 35°-45°W): (*a*) Geosat, mean seasonal cycle; (*b*) model (annual mean profile at right-hand margin); and (*c*) ship drift velocity from Figure 5 of *Richardson and McKee* [1984]; (annual mean profile at right-hand margin).

match perfectly (correlation 1.0) when the 1-month phase shift is applied.

The altimetric velocity deviations from the annual harmonic seem to indicate a nonrandom, systematic characteristic of the mean seasonal cycle: west of 54°W a relative minimum of westward anomaly in April–May is evident (more pronounced for individual years, not shown), that divides two westward maxima, in March and June. This is also seen in the contours of zonally averaged velocity anomaly in Figure 14*a*: the minimum of eastward anomaly (maximum westward) in June in the range 9°–11°N is preceded by a relative maximum in April. Westward anomalies near the coast (Figure 14*a*) are typically accompanied by eastward anomalies farther north in the latitude range 12°–18°N, suggesting at least partial coupling with the NEC and recirculation. Two maxima are also apparent in the model geostrophic boundary flow in the longitude range 54°–58°W (Figure 13*b*), and the time-latitude plot of model velocity anomalies across 54°–58°W (Figure 14*b*) compares well with those resulting from altimetry.

Finally, we compare the overall pattern of geostrophic velocity variability using eddy kinetic energy distributions based on the monthly maps (Figure 15): the model EKE shows smaller spatial scales and generally a higher level of geostrophic velocity fluctuations than the altimetry-derived EKE. In the NECC region this is obviously associated with the standing model meander pattern; zonal averaging over the meander scale results in about the same EKE level for both products. EKE estimates of *Carton and Katz* [1990], also based on monthly maps from 2 years of Geosat data, but with one-third degree meridional grid resolution, show significantly higher EKE levels in all regions: in particular, near the continental shelf in the NBC between 50°W and 55°W, EKE decreases from 700 to 300 $cm^2\ s^{-2}$. The reason for this difference is not clear. We repeated our objective analysis to resolve more small-scale variability by using a one-third

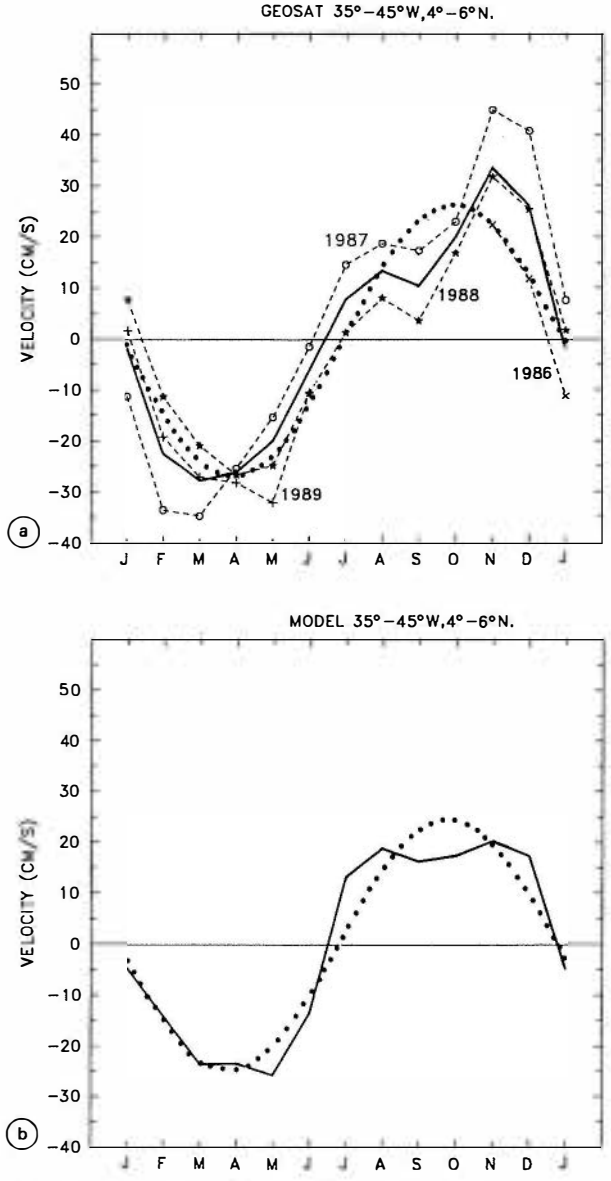

Fig. 12. Seasonal cycle (solid line) and annual harmonic (dotted line) of zonal geostrophic velocity in the NECC core (35°–45°W, 4°–6°N), for (*a*) Geosat (the individual months, November 1986 to June 1989 (dashed line), show interannual differences) and (*b*) model.

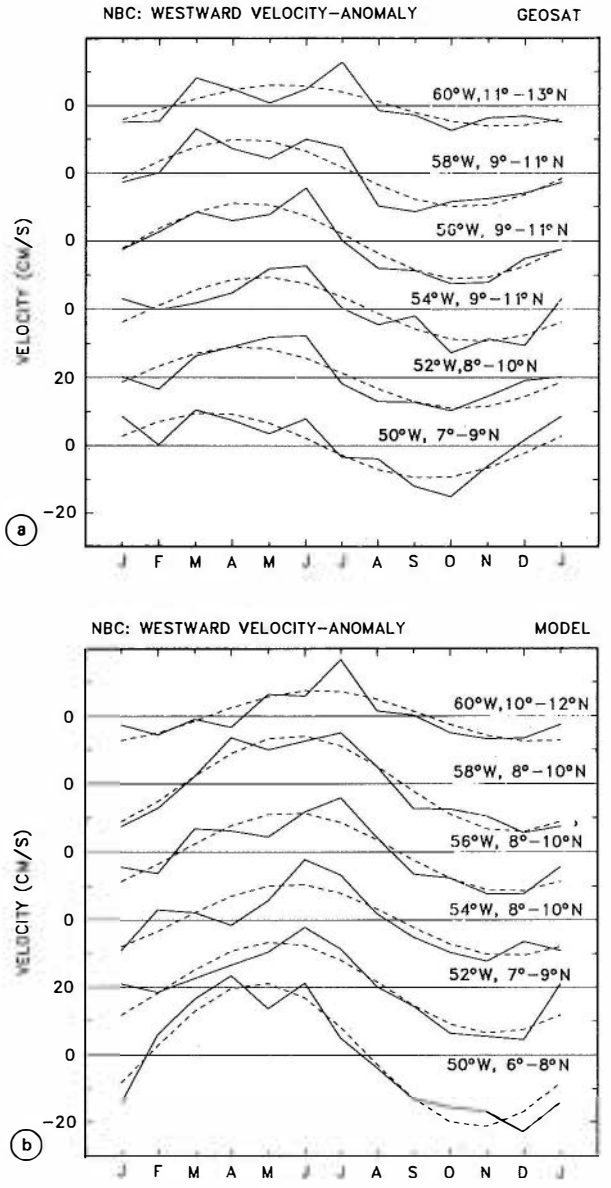

Fig. 13. Seasonal cycle (solid line) and annual harmonic (dashed line) of westward geostrophic velocity in the NBC, for sections shown in Figures 4*b* and 6, for (*a*) Geosat altimetry and (*b*) model. The westward model mean velocities for each section from 50°W to 60°W are −16, −9, −5, −4, −3, and 10 cm s^{-1}, respectively.

degree meridional grid and 150-km correlation scale; the result is an EKE level that is higher overall but still less than 200 cm^2 s^{-2} west of 50°W.

6. Summary and Conclusions

The seasonal cycles of sea surface height and geostrophic surface currents determined from 2 years of Geosat altimetry and from 1 year of a high-resolution numerical model of the western tropical Atlantic are evaluated and compared. The model SSH is taken from the surface pressure field. The model mean fields of SSH and geostrophic currents have been subtracted, and anomalies are used throughout. Since most of the variance is contained in the annual harmonic, much of the presentation and intercomparison of spatial distributions focusses on annual harmonic SSH and currents.

Total and annual harmonic SSH fluctuations of both products compare well with respect to the zonal bands of maximum variability, centered at the southern flank of the NECC and at 10°–12°N. In these regions a large fraction of the total variance (more than 60%) is explained by the annual harmonic variance. Annual cycles of thermocline depth [*Garzoli and Katz*, 1983] and of surface dynamic height [*Merle and Arnault*, 1985] are in agreement with our results with respect to the position of maximum amplitudes along 3°N at the southern flank of the western NECC (Figure 3). Along 7°N a zonal band of minimum annual SSH fluctuations of less than 3-cm amplitude defines the northern boundary of the NECC core in Geosat and model maps.

Geostrophic current ellipses of the annual harmonic com-

TABLE 1. Comparison of Geosat and Model Seasonal Cycle of Zonal Geostrophic Velocity

	Latitude Band	Root-Mean-Square Amplitude, cm s^{-1}				
		Geosat	Model	Difference	G/M	Correlation
NECC 35°–45°W						
	4°–6°N	21.2 (19.6)	19.0 (18.2)	7.0 (2.1)	1.12 (1.08)	0.95 (1.00)
NBC 54°–58°W						
Case a	8°–10°N	7.6 (7.2)	9.5 (9.1)	8.1 (6.9)	0.80 (0.79)	0.57 (0.66)
Case b	9°–11°N	8.2 (7.7)	7.3 (6.6)	7.0 (6.2)	1.12 (1.17)	0.60 (0.64)
Case c (Geosat offset 1° north)	9°–11°N (Geosat), 8°–10°N (model)			6.0 (5.1)	0.86 (0.85)	0.78 (0.83)
Case d (Geosat offset 1°north and delayed 1 month)	9°–11°N (Geosat), 8°–10°N (model)			2.5 (1.5)	0.86 (0.85)	0.97 (1.00)

G is the rms amplitude of the Geosat mean seasonal cycle, and M is that of the model seasonal cycle. Values in parentheses are for the annual harmonic cycle.

pare well for model and Geosat for the western North Equatorial Countercurrent regime, except for the pronounced meander pattern of the model NECC. Since the model meander position is almost fixed in space during July to December, the pattern is apparent in the mean flow as well. Meandering is also apparent in altimeter-derived SSH anomaly maps (see, for example, Figure 1*b*), but not at a fixed position and thus with no significant annual harmonic content. This is consistent with drifter trajectories [*Richardson and Reverdin*, 1987] in the western NECC from July to November showing propagating meanders of 900-km wavelength and with westward phase speed of 1° per month.

Meridional profiles of zonal geostrophic velocity anomalies across the western NECC regime, running from 2°N to 15°N and averaged in the longitude range 35°–45°W, show a seasonal northward migration of the eastward flowing NECC core in fall and winter from about 4°N to 6°N. The occurrence of the northward migration of zonal velocity anomalies with a phase speed of 3–4 cm s^{-1} agrees between Geosat and the model. The physics of this migration, beginning at the time of decay of local wind forcing, needs further investigation. North of the NECC core and in phase with it, a secondary weaker NECC velocity peak at about 9°N exists

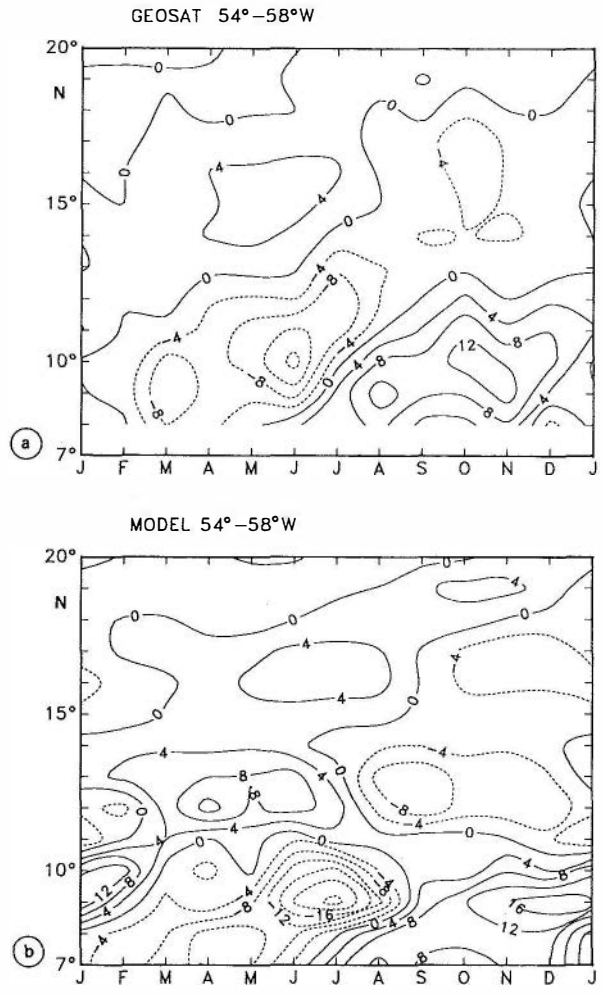

Fig. 14. Latitude-time plot of zonal geostrophic velocity anomaly in the NBC (54°–58°W): (*a*) Geosat, mean seasonal cycle; and (*b*) model, seasonal cycle.

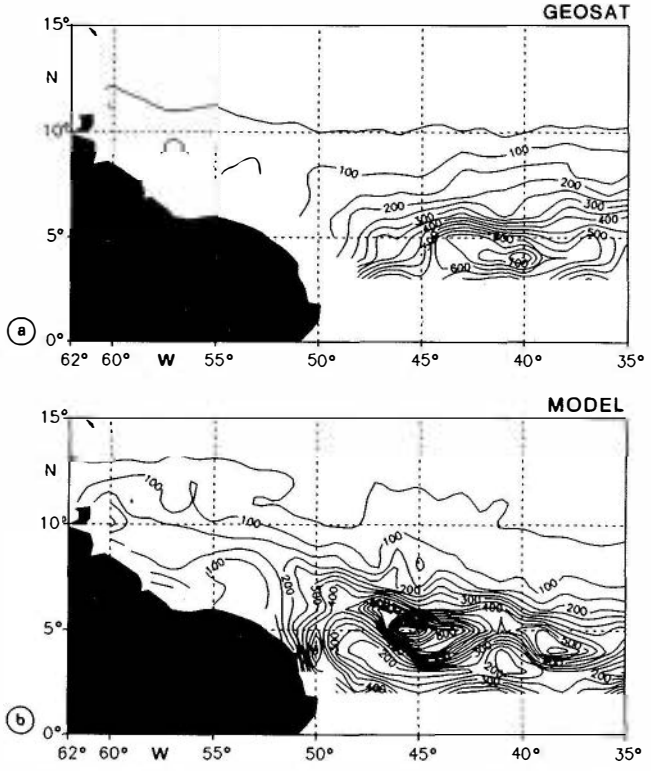

Fig. 15. Kinetic energy of geostrophic velocity fluctuations $\frac{1}{2}(\overline{u'^2} + \overline{v'^2})$: (*a*) Geosat altimetry and (*b*) model. The contour interval is 50 $cm^2\ s^{-2}$.

in both Geosat and model meridional profiles. The seasonal cycles of geostrophic velocity in the NECC core (4°–6°N) agree within 12% for the rms amplitude and are highly correlated. The model NECC core is slightly narrower, which is mainly due to interannual difference in the NECC position between the 2 averaged Geosat years. The time series of the Geosat mean seasonal cycle shows all characteristic features of the individual years, but during part of the first Geosat year (starting in November 1986) the NECC seasonal cycle is advanced in time with respect to the 2 following years. The early start of the acceleration period in March 1987 may be responsible for the large 80 cm s^{-1} difference between the seasonal minimum and maximum NECC velocities in 1987, which for the mean seasonal cycle is reduced to 60 cm s^{-1}. The 1988–1989 Geosat period shows closer agreement with the model with respect to the start of NECC acceleration in May and with respect to the seasonal minimum and maximum velocity of the NECC.

In the NBC region 50°–60°W, along the axis of maximum annual variation (Figure 7) the annual harmonic shows maximum westward geostrophic flow anomaly in April–May in the Geosat results and the annual harmonic amplitude is about 10 cm s^{-1}. In the model, maximum westward geostrophic flow occurs about one month later than in the altimetry-derived currents and the amplitude is slightly larger (except near 50°W within the retroflection region, where it is about double the Geosat amplitude). The annual amplitude derived from ship drifts (including Ekman drift currents) by *Richardson and Walsh* [1986] in the region 9°–11°N, 55°–60°W, is about 15 cm s^{-1}. Of particular interest for exploring the connection between the equatorial regime and the boundary flow near the Lesser Antilles is that there appear to be systematic deviations from the annual harmonic such that two maxima of westward flow occur for the Geosat seasonal cycle, one in March and the other in June. Indications of these two maxima can also be seen in the model currents. Further, maxima and minima of zonal flow anomalies along the western boundary appear to be associated with counter flows in the NEC belt further north, suggesting some kind of coupling between both systems.

Overall, the seasonal cycle of geostrophic surface currents from Geosat altimetry and from the WOCE CME model compare surprisingly well in the western tropical Atlantic, supplying mutual credence to both of them.

Acknowledgments. We thank D. Stammer for collaboration during development of Geosat analysis procedures, C. Böning for letting us have data from his numerical model and for helpful discussions, and E. Romaneessen for his contribution to data processing. This study has been supported by Deutsche Forschungsgemeinschaft (DFG), project SFB 133/A9.

REFERENCES

Arnault, S., Y. Menard, and J. Merle, Observing the tropical Atlantic Ocean in 1986–1987 from altimetry, *J. Geophys. Res.*, *95*(C10), 17,921–17,945, 1990.

Böning, C. W., R. Döscher, and R. G. Budich, Seasonal transport variation in the western subtropical North Atlantic: Experiments with an eddy-resolving model, *J. Phys. Oceanogr.*, *21*, 1271–1289, 1991.

Bretherton, F., R. Davis, and C. Fandry, A technique for objective analysis and design of oceanographic experiments applied to MODE-73. *Deep Sea Res.*, *23*, 559–582, 1976.

Bryan, F. O., and W. R. Holland, A high resolution simulation of the wind and thermohaline-driven circulation in the North Atlantic Ocean, Parameterization of small-scale processes, in Proceedings, 'Aha Huliko'a Hawaiian Winter Workshop, special publication, pp. 99–116, edited by P. Müller and D. Henderson, Hawaii Inst. of Geophys., Honolulu, 1989.

Carton, J. A., Estimates of sea level and current in the tropical Atlantic Ocean using Geosat altimetry, *J. Geophys. Res.*, *94*(C6), 8029–8039, 1989.

Carton, J. A., and E. J. Katz, Estimates of the zonal slope and seasonal transport of the Atlantic North Equatorial Countercurrent, *J. Geophys. Res.*, *95*(C3), 3091–3100, 1990.

Cheney, R. E., J. G. Marsh, and B. D. Beckley, Global mesoscale variability from collinear tracks of Seasat altimeter data, *J. Geophys. Res.*, *88*(C7), 4343–4354, 1983.

Cheney, R. E., B. C. Douglas, R. W. Miller, D. L. Porter, and N. S. Doyle, Geosat altimeter geophysical data record user handbook, *NOAA Tech. Memo. NOS NGS-46*, Natl. Ocean Serv., Rockville, Md., 1987.

Cheney, R. E., B. C. Douglas, and L. Miller, Evaluation of Geosat altimeter data with application to tropical Pacific sea level variability, *J. Geophys. Res.*, *94*(C4), 4737–4748, 1989.

De Mey, P., and Y. Menard, Synoptic analysis and dynamical adjustment of GEOS 3 and Seasat altimeter eddy fields in the northwest Atlantic, *J. Geophys. Res.*, *94*(C5), 6221–6231, 1989.

Emery, W. J., G. H. Born, D. G. Baldwin, and C. L. Norris, Satellite-derived water vapor corrections for Geosat-altimetry, *J. Geophys. Res.*, *95*(C3), 2953–2964, 1990.

Garzoli, S. L., and E. J. Katz, The forced annual reversal of the Atlantic North Equatorial Countercurrent, *J. Phys. Oceanogr.*, *13*, 2082–2090, 1983.

Hellerman, S., and M. Rosenstein, Normal monthly wind stress over the world ocean with error estimates, *J. Phys. Oceanogr.*, *13*, 1093–1104, 1983.

Marsh, J. G., R. E. Cheney, J. J. McCarthy, and T. V. Martin, Regional mean sea surfaces based upon GEOS 3 and Seasat altimeter data, *Mar. Geod.*, *8*, 385–402, 1984.

Menard, Y., Observing the seasonal variability in the tropical Atlantic from altimetry, *J. Geophys. Res.*, *93*(C11), 13,967–13,978, 1988.

Merle, J., and S. Arnault, Seasonal variability of the surface dynamic topography in the tropical Atlantic Ocean, *J. Mar. Res.*, *43*, 267–288, 1985.

Miller, L., and R. Cheney, Large-scale meridional transport in the tropical Pacific Ocean during the 1986–1987 El Niño from Geosat, *J. Geophys. Res.*, *95*(C10), 17,905–17,919, 1990.

Philander, G., and R. C. Pacanowski, A model of the seasonal cycle in the Tropical Atlantic Ocean, *J. Geophys. Res.*, *91*(C12), 14192–14206, 1986.

Richardson, P. L., and T. K. McKee, Average seasonal variation of the Atlantic equatorial currents from historical ship drifts, *J. Phys. Oceanogr.*, *14*, 1226–1238, 1984.

Richardson, P. L., and G. Reverdin, Seasonal cycle of velocity in the Atlantic North Equatorial Countercurrent measured by surface drifters, current meters and ship drifts, *J. Geophys. Res.*, *92*(C4), 3691–3708, 1987.

Richardson, P. L., and D. Walsh, Mapping climatological seasonal variations of surface currents in the tropical Atlantic using ship drifts, *J. Geophys. Res.*, *91*(C9), 10,537–10,550, 1986.

Schott, F., and C. W. Böning, The WOCE model in the western equatorial Atlantic: Upper layer circulation, *J. Geophys. Res.*, *96*(C4), 6993–7004, 1991.

N. Didden and F. Schott, Institut für Meereskunde an der Universität Kiel, Düsternbrooker Weg 20, 2300 Kiel 1, Germany.

(Received November 12, 1990;
revised June 3, 1991;
accepted October 16, 1991.)